A Bpp-based Dinuclear Ruthenium Photocatalyst for Visible Light-Driven Oxidation Reactions

Seán Hennessey[a], Pau Farràs[a,b*], Jordi Benet-Buchholz[c], Antoni Llobet[b,c*]

Supporting Information

a. School of Chemistry, Energy Research Centre, Ryan Institute, National University of Ireland, Galway (NUI Galway), University Road, H91 CF50 Galway, Ireland.
b. Institute of Chemical Research of Catalonia (ICIQ), Av. Països Catalans 16, 43007 Tarragona, Spain.
c. Departament de Química, Universidad Autònoma de Barcelona, Cerdanyola del Vallès, 08193 Barcelona, Spain.
*Correspondence: pau.farras@nuigalway.ie; Tel.: +353 91 492765 (P.F.); allobet@iciq.es; Tel.: +34 977 920 000 (A.L.).

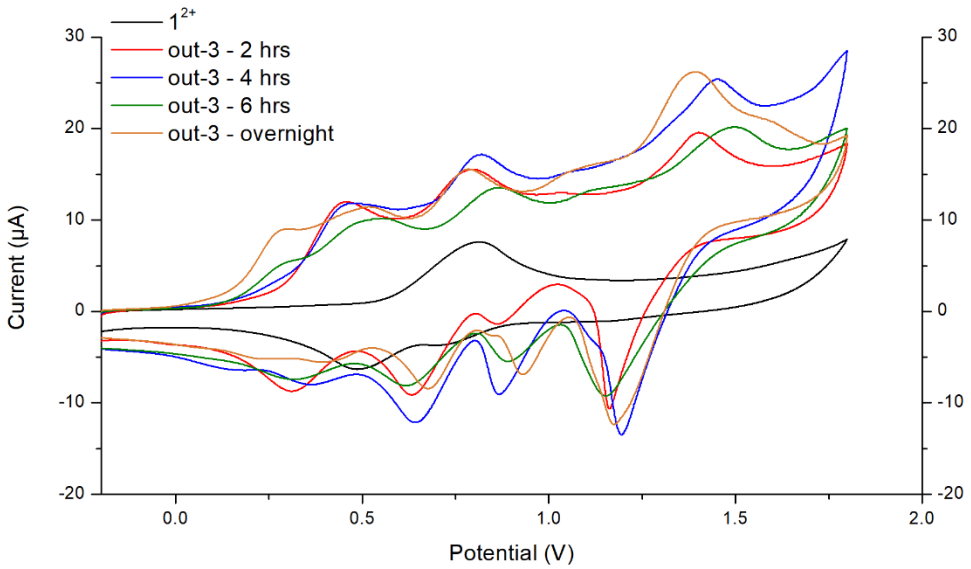

Figure S1: Cyclic voltammograms of ***out*-[3-Cl]$^{2+}$** showing degradation under ambient light over time periods of 2 hours in CH_2Cl_2, scan rate 0.1 V/s. *out*-[**1**]$^{2+}$ shown for comparison.

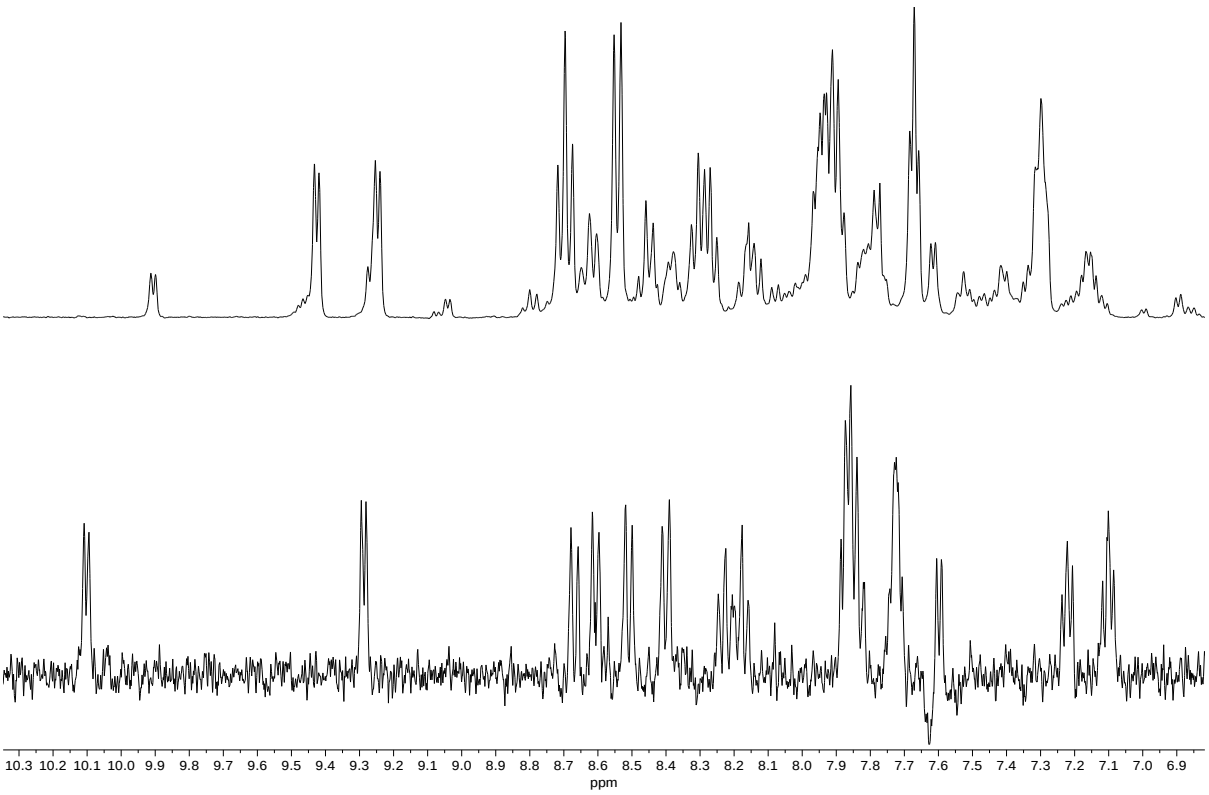

Figure S2: Stacked ^{1}H-NMR spectra of impure ***out*-[3-Cl]$^{2+}$** before light irradiation (above) and after light irradiation (below) performed in MeOD. Apodization for bottom spectra: Exponential: 1.60 Hz, Integral-to-noise effect : 5.129 s.

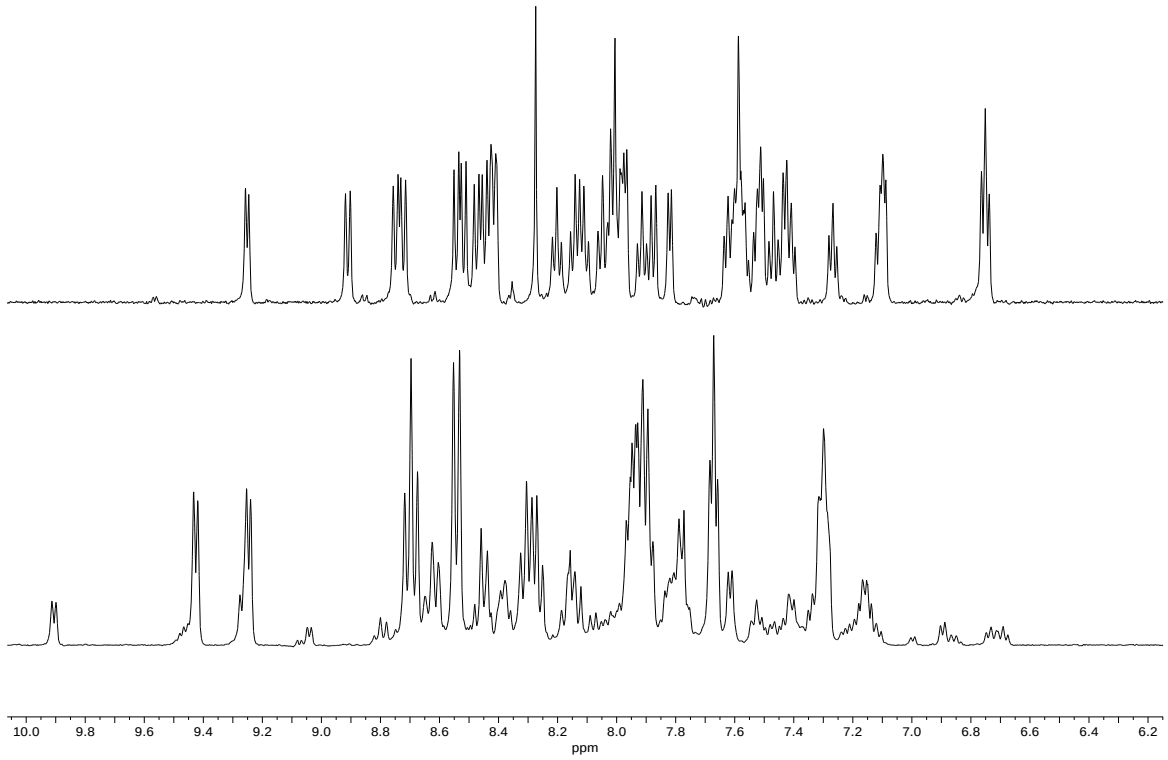

Figure S3: Stacked ^{1}H-NMR spectra of ***in*-[3-Cl]$^{2+}$** in $(CD_3)_2CO$ (above) and impure ***out*-[3-Cl]$^{2+}$** before light irradiation performed in MeOD (below).

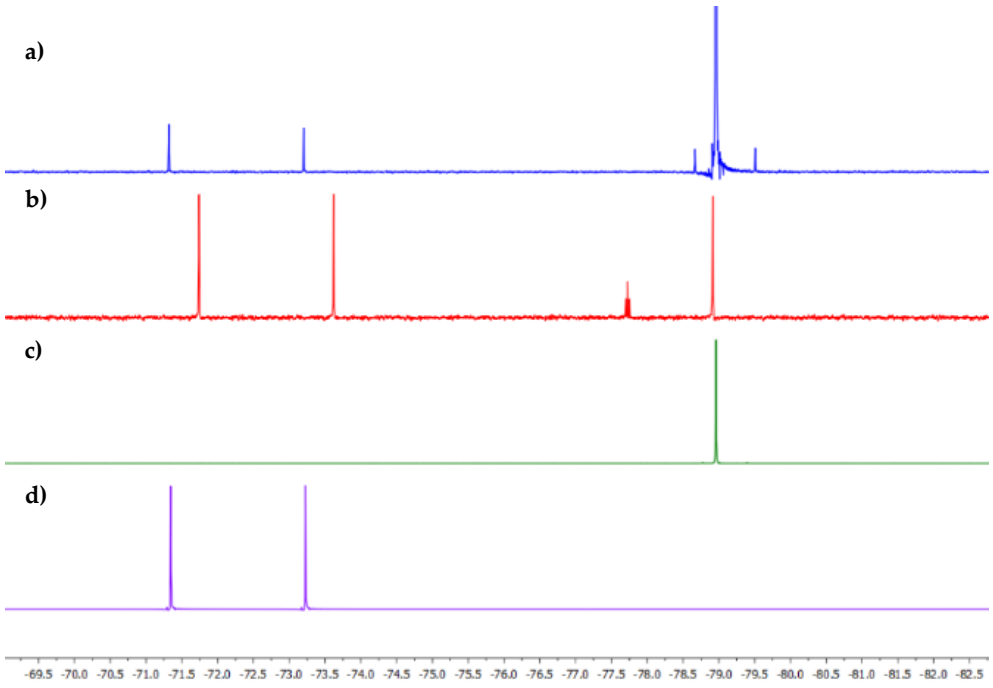

Figure S4: ^{19}F NMR comparisons between; a) ***in*-[3-OH$_2$]$^{3+}$** in D_2O b) ***in*-[3-OCOCF$_3$]$^{2+}$** in acetone-d_6. The ^{19}F NMR of free trifluoroacetate in D_2O (c) and free potassium hexafluorophosphate in D_2O (d) are shown for comparison

Table S1. Crystallographic data for complexes ***in*-[3-L](PF$_6$)$_{2/3}$** where; L = CH_3CN or Cl.

	***in*-[(bpy)$_2$Ru(bpp)Ru(CH_3CN)(tpy)](PF$_6$)$_3$**	***in*-[(bpy)$_2$Ru(bpp)Ru(Cl)(tpy)](PF$_6$)$_2$**
Empirical formula	$C_{50}H_{39}F_{18}N_{12}P_3Ru_2$	$C_{51}H_{42}ClF_{12}N_{11}OP_2Ru_2$
M_r (g mol^{-1})	1444.98	1352.48
Crystal system	Triclinic	Triclinic
Space group	P-1	P-1
a [Å]	10.6161(10)	12.9180(4)
b [Å]	15.1085(13)	13.8310(4)
c [Å]	16.9110(14)	17.5520(6)
α [°]	90.103(3)	92.9970(19)
β [°]	94.853(2)	100.953(2)
γ [°]	105.573(2)	105.6680(18)
Volume [Å^3]	2602.6(4)	2946.61(16)
Z	2	2
ρ_{calcd} [Mg/m^3]	1.844	1.524
Absorption coefficient [mm^{-1}]	0.789	0.696
Final R indices [I>2σ(I)]	R_1 = 0.0412 , wR_2 = 0.0925	R_1 = 0.0771, wR_2 = 0.2103
R indices (all data)	R_1 = 0.0604 , wR_2 = 0.1014	R_1 = 0.1404, wR_2 = 0.2549

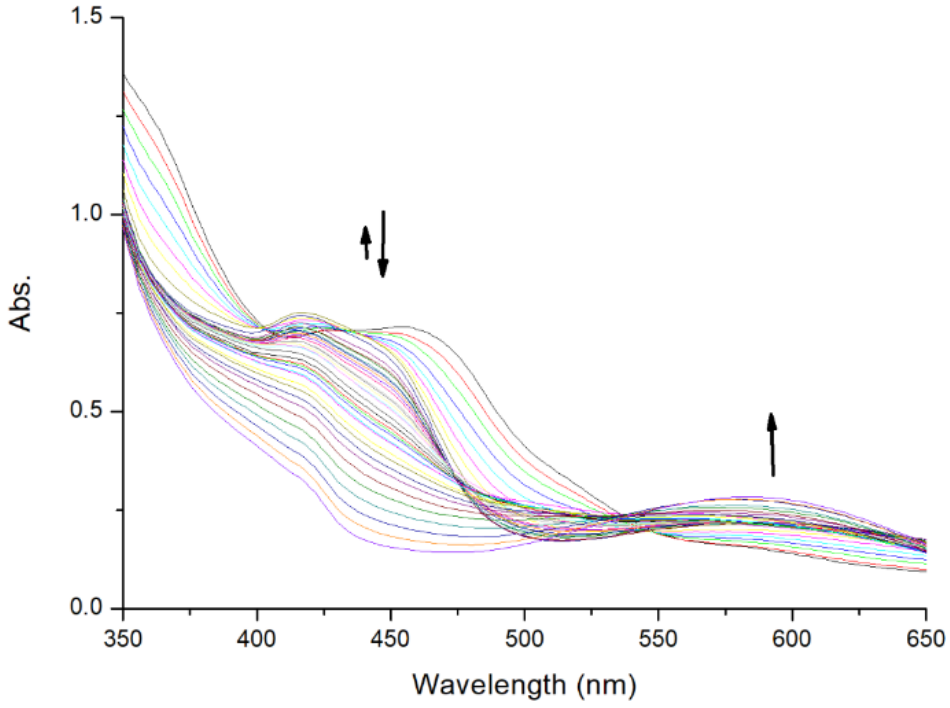

Figure S5: UV-vis redox titration of ***in*-[3-OH$_2$]$^{3+}$** at pH = 1, upon addition of 0.1 eq. (up to 4 eq.) of Ce(IV) over time.

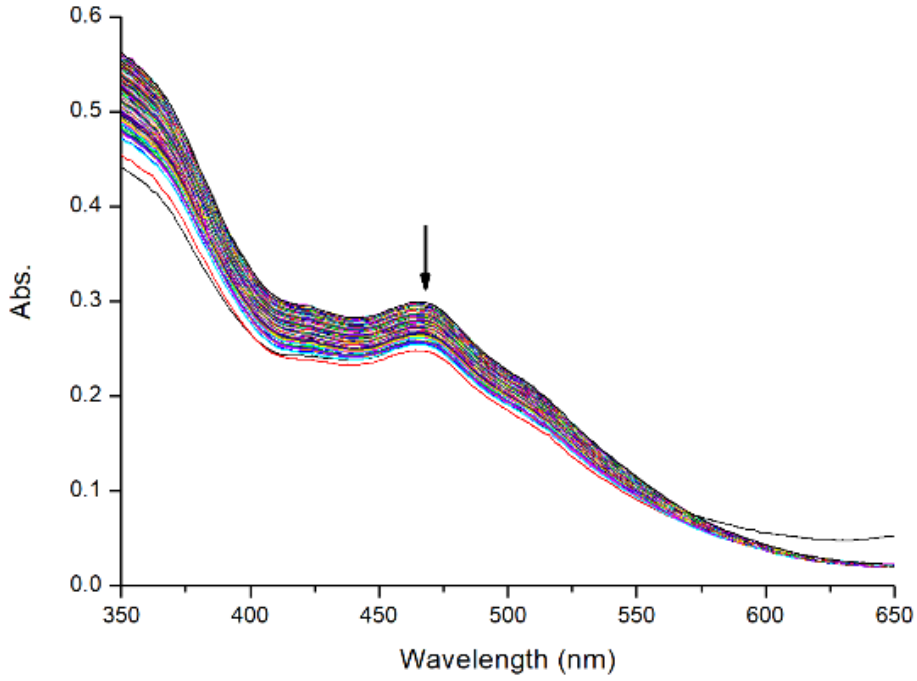

Figure S6: UV-Vis absorbance spectra over time for an aqueous solution of ***in*-[3-OH]3^{+}** at pH = 12 under air. The arrow indicates the decrease in absorption at the MLCT as a result of precipitation of the complex.

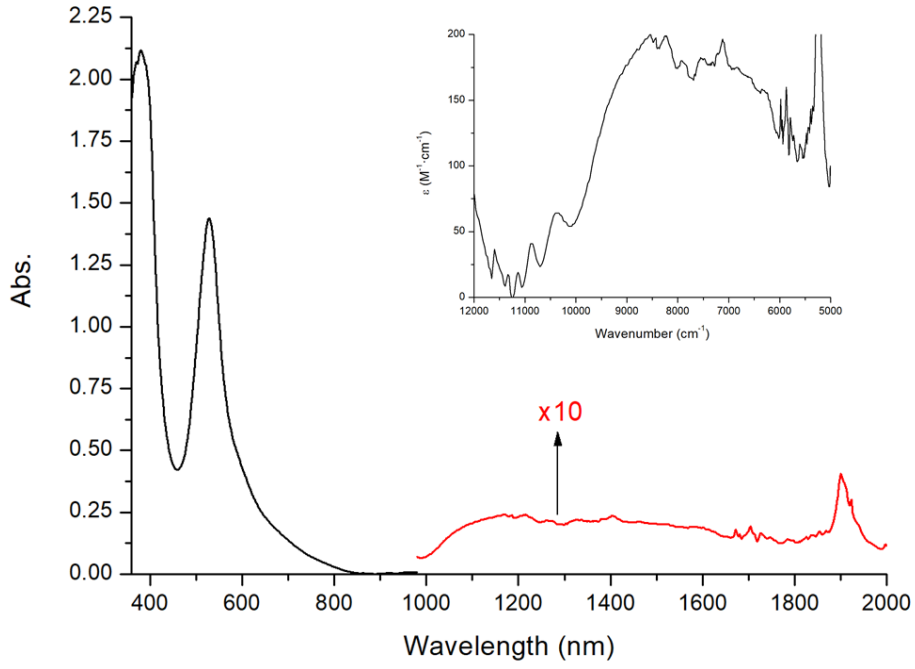

Figure S7: Vis-NIR spectra of ***in*-[3-OH$_2$]$^{3+}$** in CF_3SO_3H (pH = 1). Values between 1000-2000 nm multiplied by 10 for visibility. Inset: Vis-NIR spectra of ***in*-[3-OH$_2$]$^{3+}$** in CF_3SO_3H (pH = 1) at a concentration of 2.0 mM. ν_{max} (cm^{-1}) = 8422.

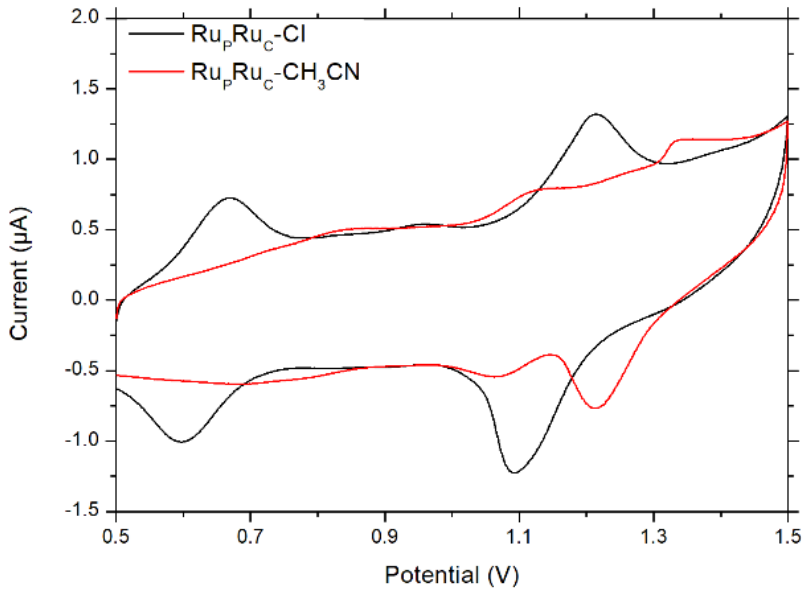

Figure S8: Cyclic voltammograms of ***in*-[3-Cl]$^{2+}$** and ***in*-[3-CH$_3$CN]$^{3+}$** in a deoxygenated solution of CH_2Cl_2 with supporting electrolyte TBAF (0.1 M) scan rate of 0.01 Vs^{-1}.

Table S2: NMR spectroscopy data

Complex	**1D NMR data**
***In*-[3-Cl]$^{2+}$**	^{1}H NMR (400 MHz, $(CD_3)_2CO$)) δ 9.25 (d, *J* = 5.6 Hz, 1H), 8.91 (d, *J* = 8.1 Hz, 1H), 8.74 (dd, *J* = 13.1, 8.1 Hz, 2H), 8.56 – 8.40 (m, 6H), 8.27 (s, 1H), 8.20 (t, *J* = 7.5 Hz, 1H), 8.13 (dt, *J* = 15.0, 7.8 Hz, 2H), 8.07 – 7.95 (m, 5H), 7.93 – 7.86 (m, 2H), 7.82 (d, *J* = 5.9 Hz, 1H), 7.64 – 7.39 (m, 9H), 7.27 (t, *J* = 6.8 Hz, 1H), 7.10 (dd, *J* = 11.0, 5.9 Hz, 2H), 6.75 (t, *J* = 6.7 Hz, 2H). ^{13}C-NMR (101 MHz, $(CD_3)_2CO$) δ: 160.30, 159.39, 158.86, 158.71, 158.57, 157.75, 156.92, 156.86, 156.32, 156.07, 155.87, 155.03, 154.85, 154.49, 152.94, 152.01, 151.96, 150.87, 150.78, 150.73, 150.39, 137.57, 137.22, 136.63, 136.48, 135.62, 135.37, 135.32, 132.31, 127.43, 127.42, 126.64, 126.56, 125.60, 124.65, 124.14, 123.28, 123.24, 123.11, 122.98, 122.52, 122.36, 122.15, 121.71, 120.91, 119.69, 104.44
***In*-[3-CH$_3$CN]$^{3+}$**	^{1}H-NMR (400 MHz, CD_3CN) δ: 8.76 (dt, *J* = 5.5, 1.3 Hz, 1H), 8.64 – 8.49 (m, 3H), 8.41 (ddd, *J* = 18.7, 8.1, 0.9 Hz, 2H), 8.33 – 8.25 (m, 3H), 8.19 (q, *J* = 7.9 Hz, 2H), 8.13 – 7.98 (m, 5H), 7.97 (s, 1H), 7.84 – 7.73 (m, 2H), 7.61 (td, 2H), 7.56 – 7.34 (m, 6H), 7.29 (ddd, *J* = 7.4, 5.7, 1.3 Hz, 1H), 7.24 – 7.17 (m, 3H), 7.12 (ddd, *J* = 7.3, 5.6, 1.3 Hz, 1H), 6.95 (ddt, *J* = 5.8, 1.5, 0.8 Hz, 1H), 6.90 (ddt, 1H), 6.75 (ddt, 1H). (35 protons?) ^{13}C-NMR (101 MHz, CD_3CN) δ: 158.82, 158.46, 158.18, 157.84, 157.65, 157.38, 157.30, 155.83, 155.56, 154.85, 154.17, 153.84, 152.61, 152.15, 151.84, 151.13, 150.94, 149.85, 138.53, 137.94, 137.86, 137.66, 137.46, 136.92, 136.43, 136.27, 128.50, 127.56, 127.22, 127.19, 126.17, 125.37, 124.77, 124.53, 124.33, 124.03, 123.96, 123.59, 123.36, 123.29, 122.99, 121.35, 120.09, 104.50.
***In*-[3-OH$_2$]$^{3+}$**	^{1}H NMR (400 MHz, D_2O) δ 8.42 (dd, J = 7.0, 5.1 Hz, 2H), 8.38 – 8.12 (m, 8H), 8.06 – 7.82 (m, 11H), 7.76 (m, 1H), 7.69 (d, J = 8.1 Hz, 1H), 7.51 (m, 2H), 7.42 – 7.29 (m, 6H), 7.15 (ddd, J = 7.3, 5.7, 1.3 Hz, 2H), 7.01 (s, 1H), 6.84 (s, 1H), 6.71 (s, 1H), 6.65 (ddd, J = 7.3, 5.7, 1.3 Hz, 1H), 6.50 (t, J = 6.6 Hz, 1H).

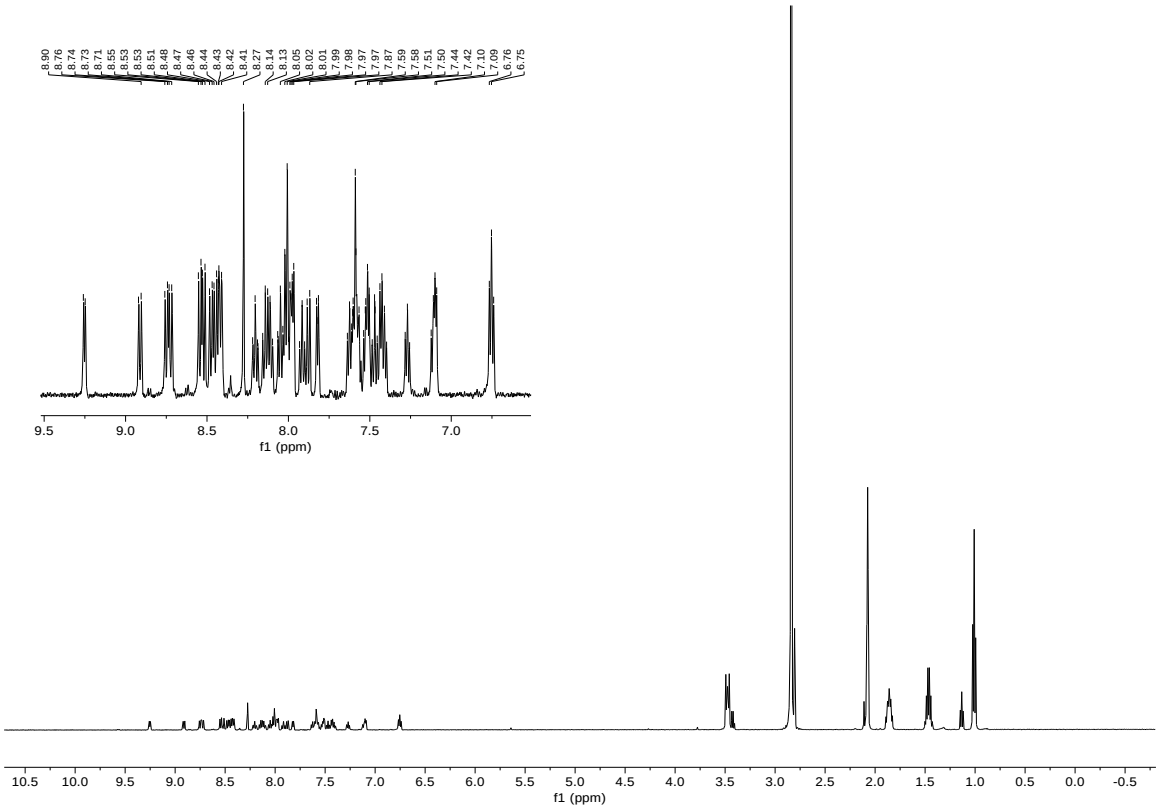

Figure S9: ^{1}H-NMR spectrum of ***in*-[3-Cl]$^{2+}$** performed in $(CD_3)_2CO$.

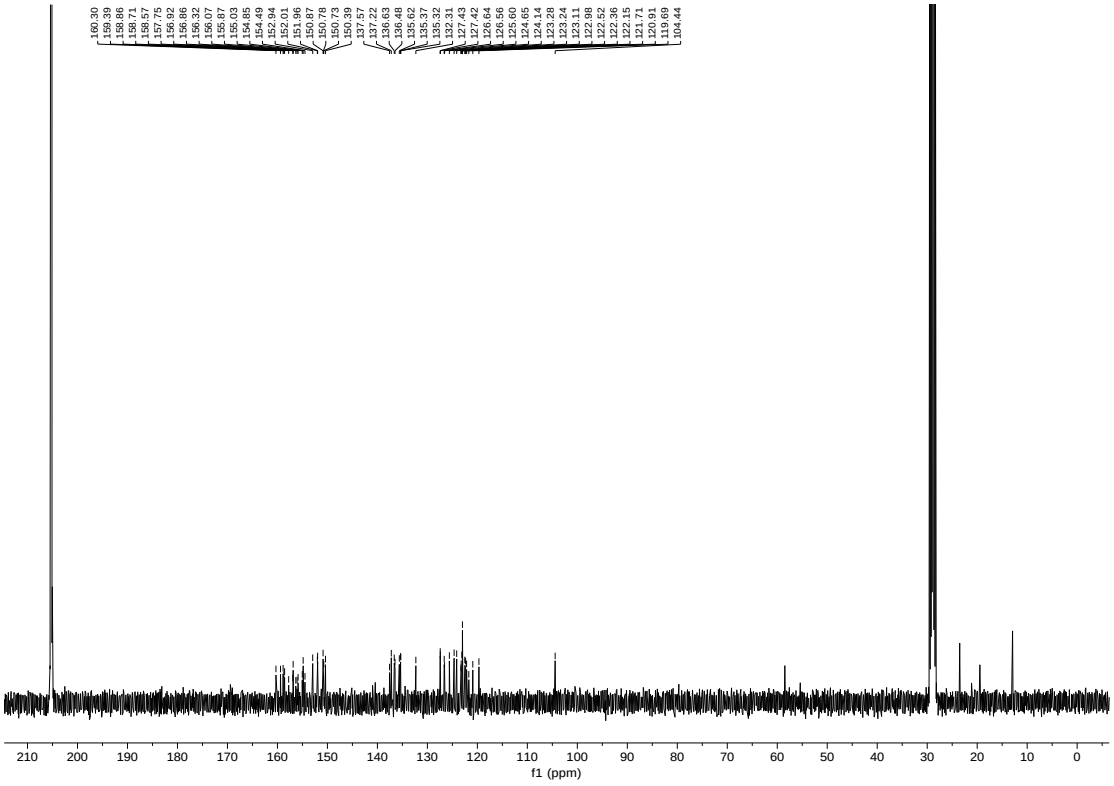

Figure S10: ^{13}-CMR spectrum of ***in*-[3-Cl]$^{2+}$** performed in $(CD_3)_2CO$.

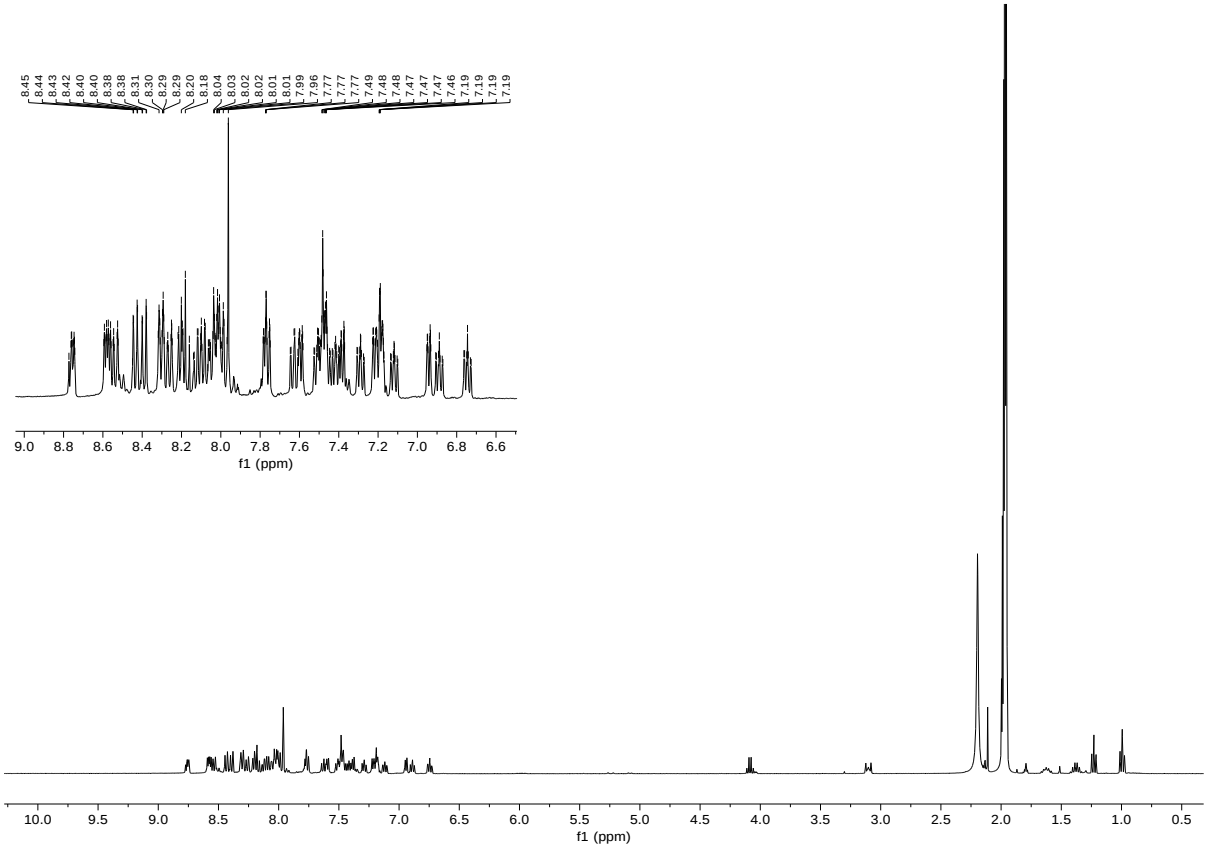

Figure S11: ^{1}H-NMR spectrum of ***in*-[3-CH$_3$CN]$^{3+}$** performed in CD_3CN.

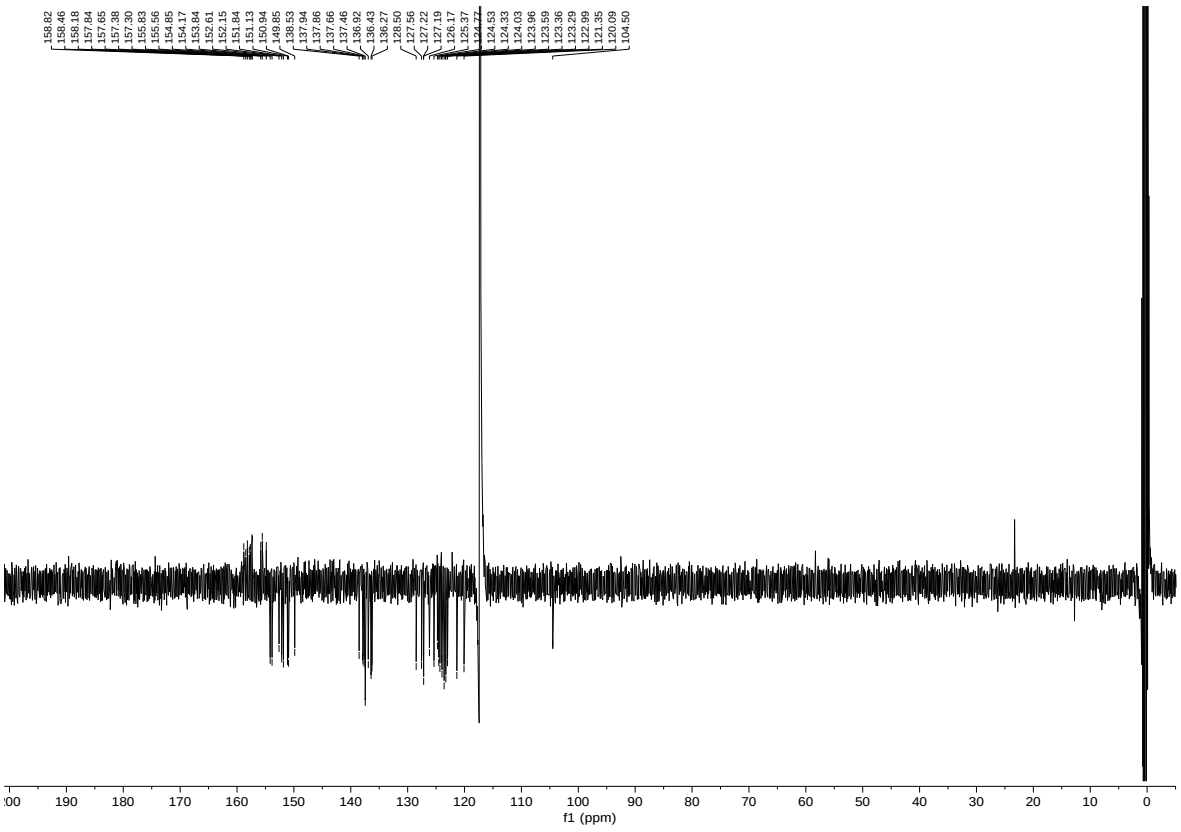

Figure S12: DEPT spectrum of ***in*-[3-CH$_3$CN]$^{3+}$** performed in CD_3CN.

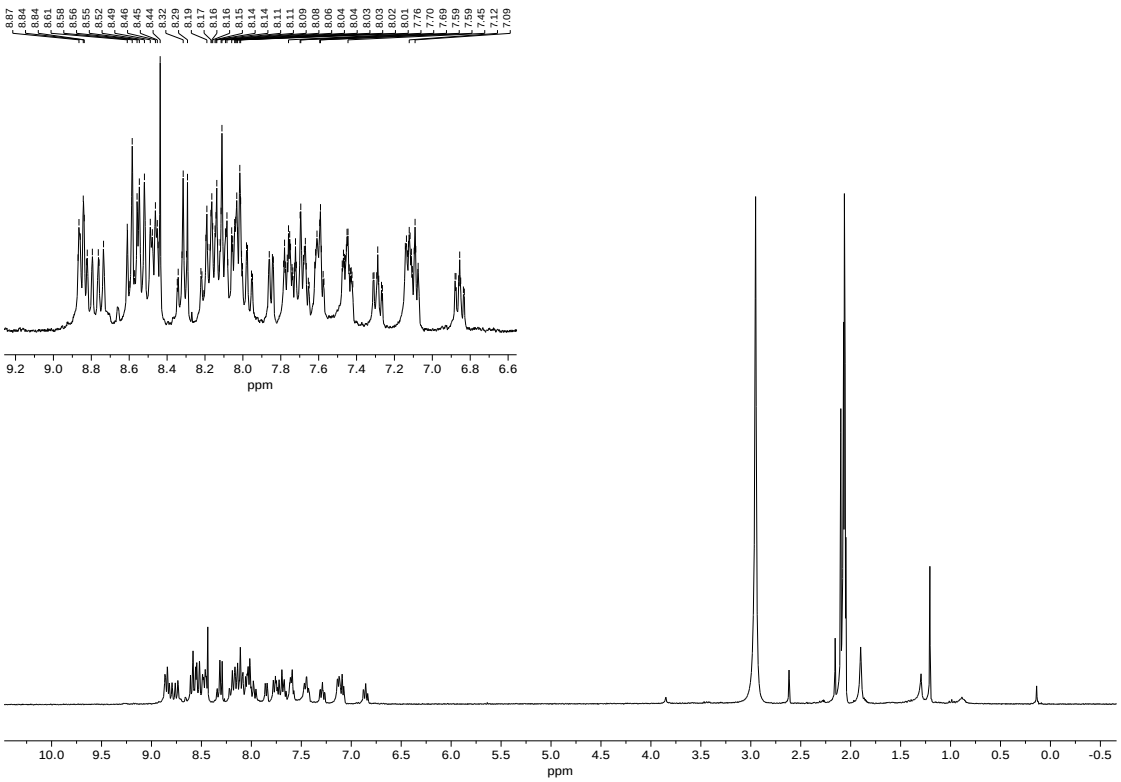

Figure S13: ^{1}H-NMR spectrum of ***in*-[3-OOCCF$_3$]$^{2+}$** performed in $(CD_3)_2CO$.

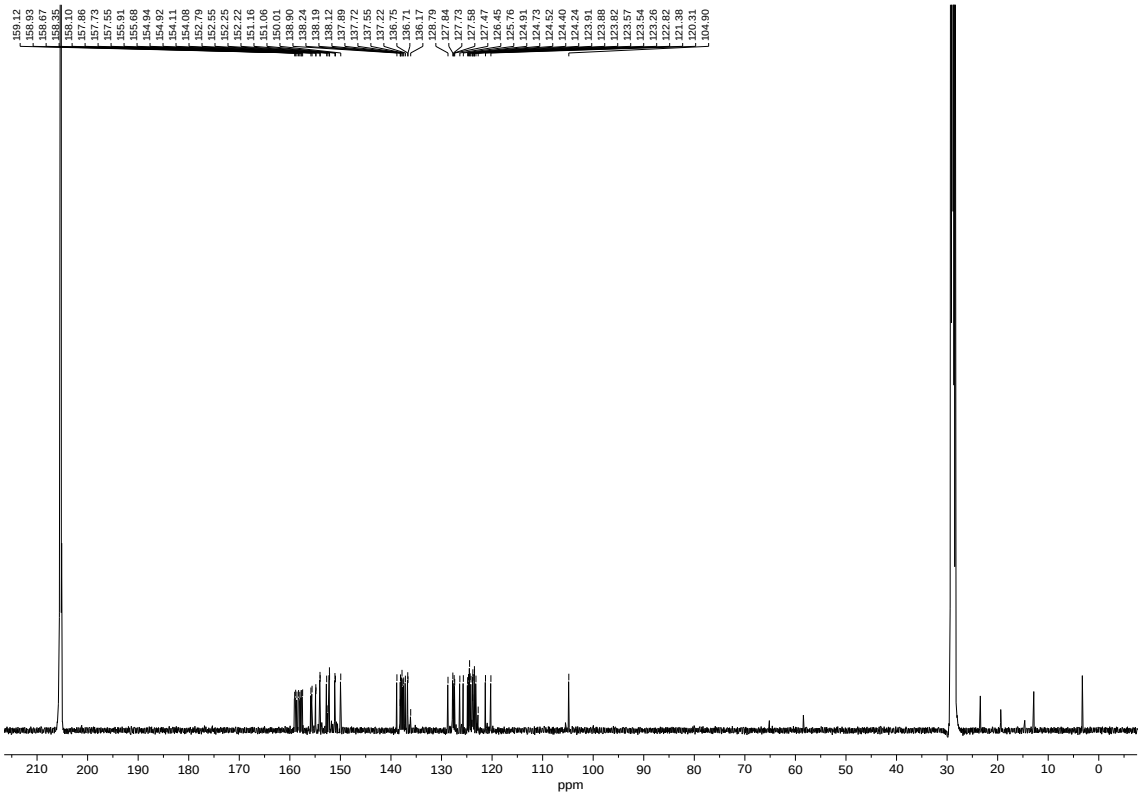

Figure S14: ^{13}C-NMR spectrum of ***in*-[3-OOCCF$_3$]$^{2+}$** performed in $(CD_3)_2CO$.

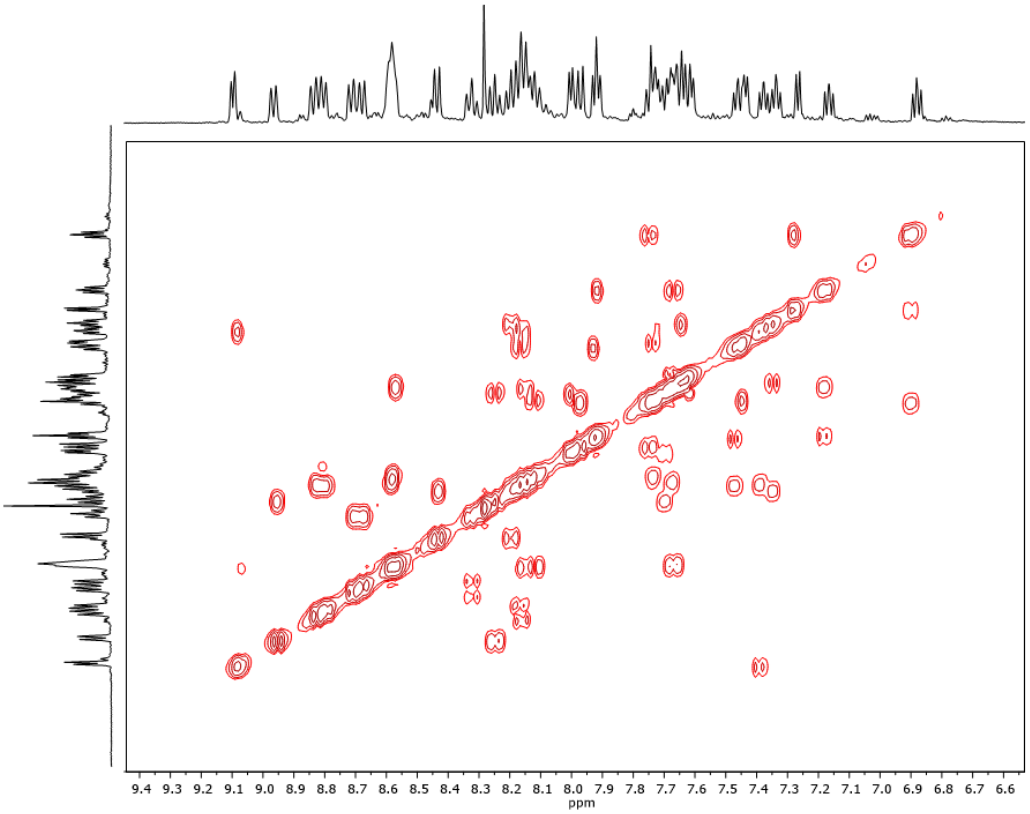

Figure S15: COSY spectrum of ***in*-[3-OOCCF$_3$]$^{2+}$** performed in $(CD_3)_2CO$.

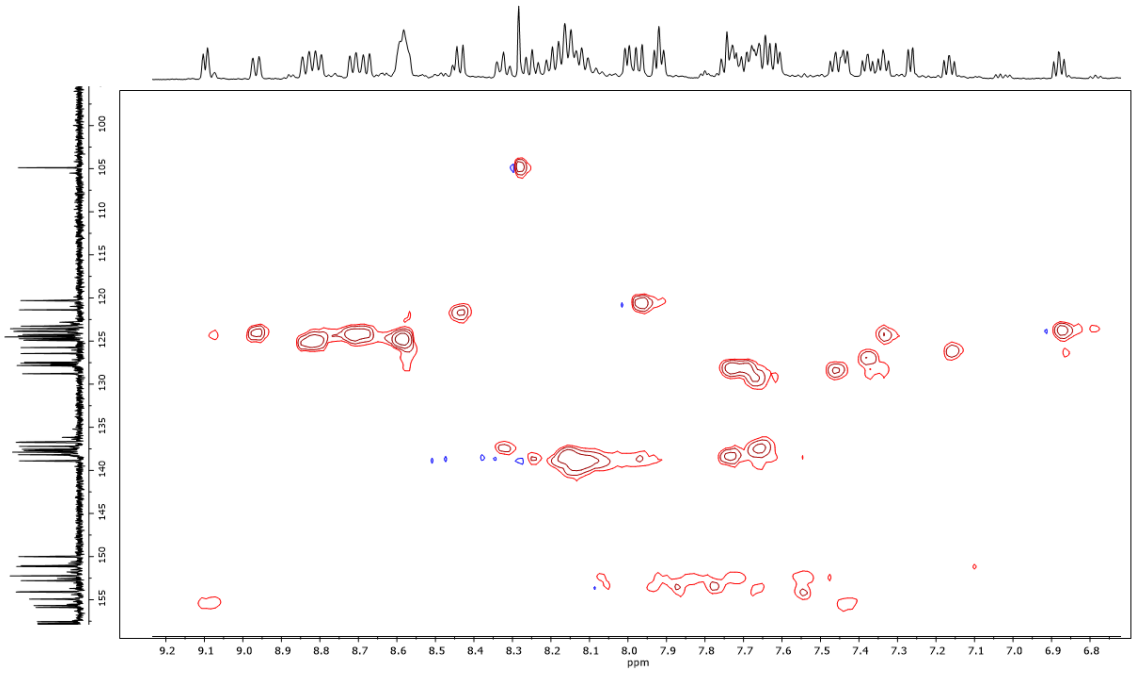

Figure S16: HSQC spectrum of ***in*-[3-OOCCF$_3$]$^{2+}$** performed in $(CD_3)_2CO$.

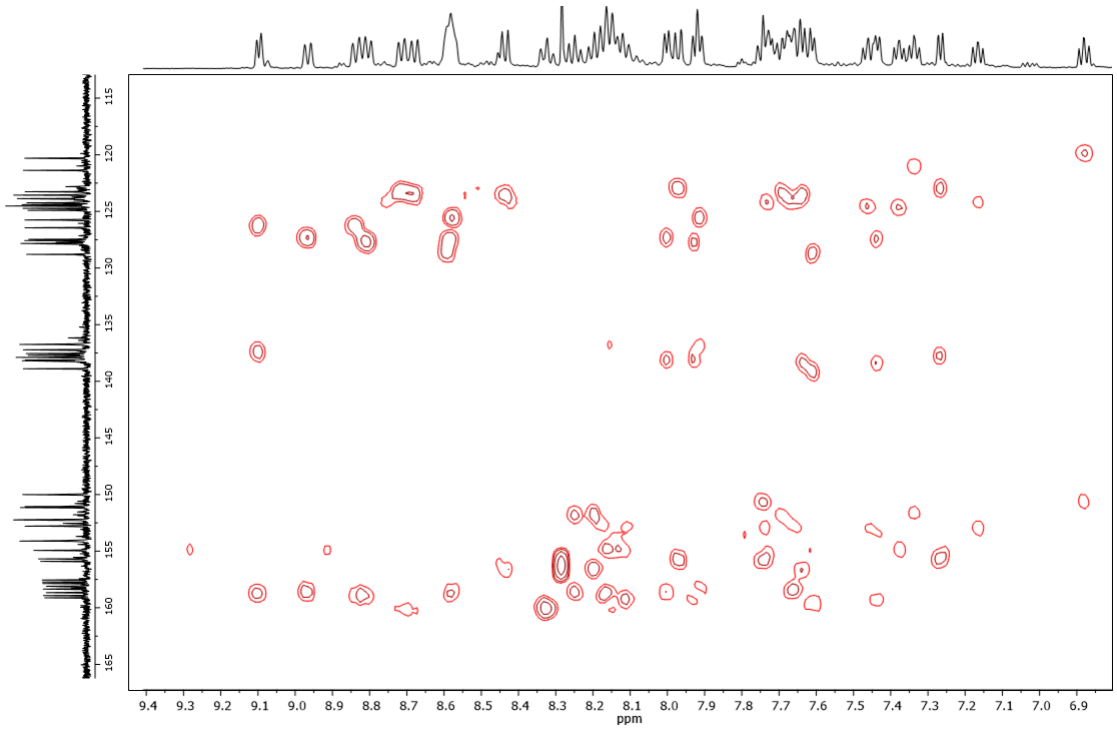

Figure S17: HMBC spectrum of ***in*-[3-OOCCF$_3$]$^{2+}$** performed in $(CD_3)_2CO$.

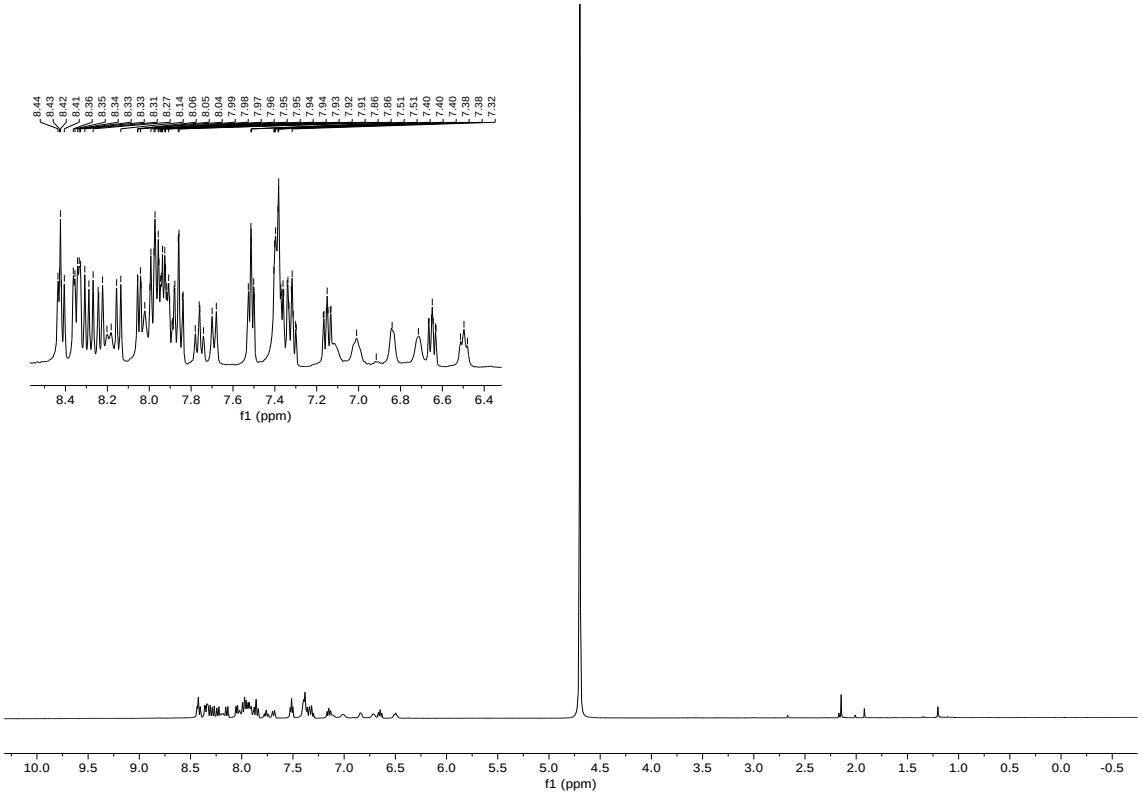

Figure S18: ^{1}H-NMR of ***in*-[3-OH$_2$]$^{3+}$** in D_2O.

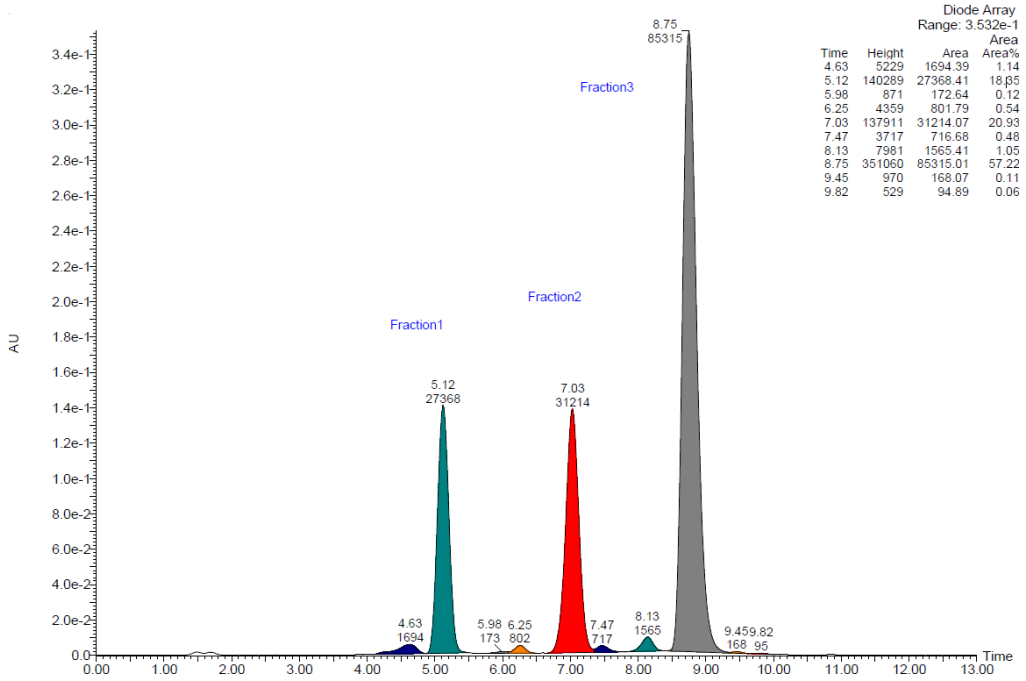

Figure S19: Full HPLC chromatogram of dyad mixture after reaction (iv). Fractions assigned by mass spec. Fraction 1 - $Ru(tpy)_2$ derivative, Fraction 2 – $\mathbf{2^{2+}}$, Fraction 3 – ***in*-[3-OCOCF$_3$]$^{2+}$**.

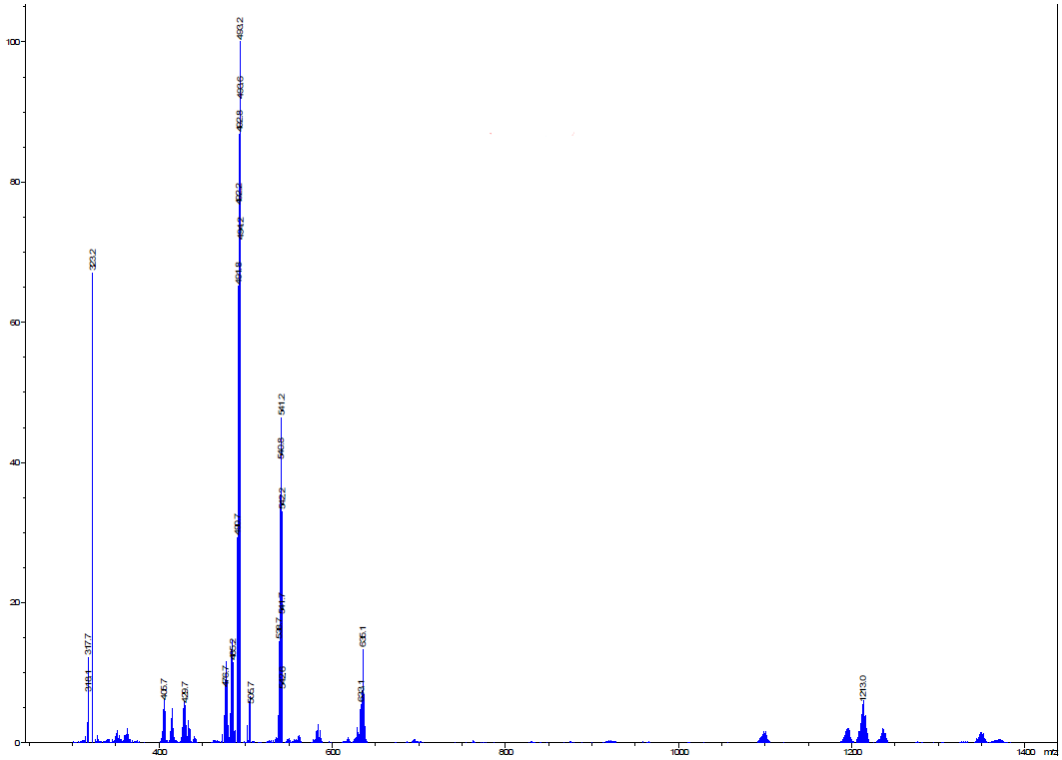

Figure S20: ESI-MS of pure fraction from HPLC dissolved in H_2O to give, ***in*-[3-OH$_2$]$^{3+}$**, performed in MeOH with the addition of H_2O. m/z (M^{3+}) = 493.2.

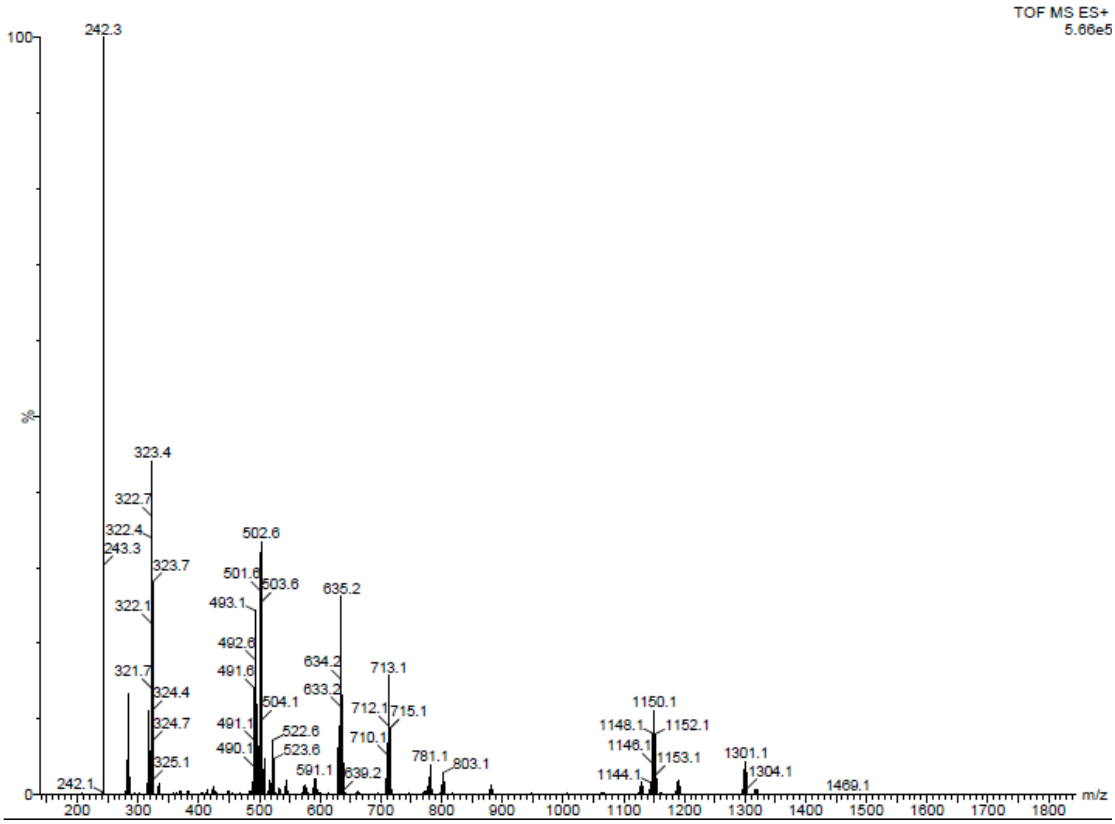

Figure S21: ESI-MS of ***in*-[3-CH_3CN]$^{3+}$** performed in MeOH with the addition of H_2O.

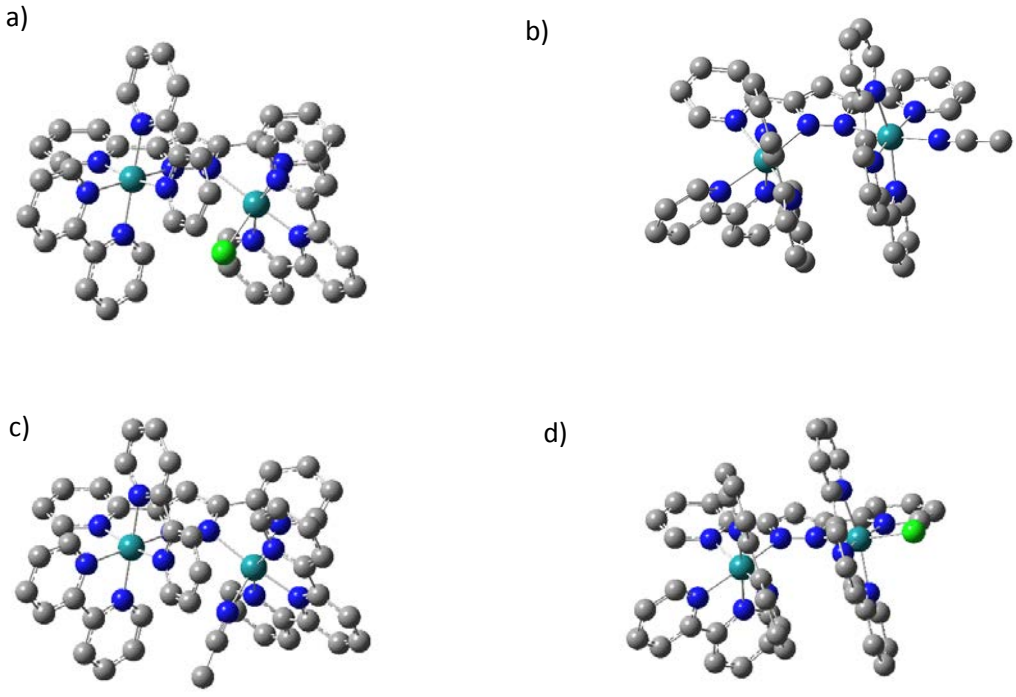

Figure S22: DFT optimized structures of (a) ***in*-[3-Cl]$^{2+}$** (b) ***out*-[3-Cl]$^{2+}$** (c) ***in*-[3-CH_3CN]$^{3+}$** (d) ***out*-[3-CH_3CN]$^{3+}$**. Hydrogen atoms are omitted for clarity.